Ilamycin E and ilamycin F are dual inhibitors of ClpX and ClpC1 in mycobacteria

Authors

Yamin Gao[1,2,3,4,†], Cuiting Fang[1,2,3,4,†], Biao Zhou[1,5,6], H.M. Adnan Hameed[1,2,3,4], Changli Sun[3,7], Xirong Tian[1,2,3,4], Jing He[1,2,4,8], Xingli Han[1,2,3,4], Han Zhang[1,2,4,9], Jun Li[10], Jianhua Ju[3,7], Xinwen Chen[6], Nanshan Zhong[6], Junying Ma[3,7,*], Xiaoli Xiong[1,2,3,6,*], Tianyu Zhang[1,2,3,4,6,*]

Affiliations

[1]State Key Laboratory of Respiratory Disease, Guangzhou Institutes of Biomedicine and Health, Chinese Academy of Sciences, Guangzhou 510530, China.

[2]Guangdong-HongKong-Macau Joint Laboratory of Infectious Respiratory Diseases, Guangzhou Institutes of Biomedicine and Health, Chinese Academy of Sciences, Guangzhou 510530, China.

[3]University of Chinese Academy of Sciences, Beijing 100049, China.

[4]China-New Zealand Belt and Road Joint Laboratory on Biomedicine and Health, Guangzhou Institutes of Biomedicine and Health, Chinese Academy of Sciences, Guangzhou 510530, China.

[5]Guangzhou Medical University, Guangzhou 510180, China.

[6]Guangzhou National Laboratory, Guangzhou 510005, China.

[7]CAS Key Laboratory of Tropical Marine Bio-Resources and Ecology, Guangdong Key Laboratory of Marine Materia Medica, RNAM Center for Marine Microbiology, South China Sea Institute of Oceanology, Chinese Academy of Sciences, Guangzhou 510301, China.

[8]Institute of Physical Science and Information Technology, Anhui University, Hefei 230601, China.

[9]School of Life Sciences, University of Science and Technology of China, Hefei 230026, China.

[10]Shanghai Institute for Advanced Immunochemical Studies and School of Life Science and Technology, ShanghaiTech University, Shanghai 201210, China.

[†]These authors contributed equally to this work.

[*]Correspondence: majunying@scsio.ac.cn (J. Ma), xiong_xiaoli@gibh.ac.cn (X. Xiong), zhang_tianyu@gibh.ac.cn (T. Zhang)

Running head

Ilamycin E/F are inhibitors of mycobacterial ClpX/ClpC1

Abstract

Mycobacterial caseinolytic protease (Clp) proteolytic system has emerged as a promising therapeutic target. Numerous natural cyclic peptides, like ilamycins, have been reported to possess antitubercular activities by targeting ClpC1 component of the ClpC1P1P2 proteasome, albeit without strong genetic evidence. Here, we discovered that ilamycin E (ILE) and ilamycin F (ILF) exhibit more potent delayed mycobactericidal activities than other ilamycin components. Novel insertion mutations in *clpC1* and a unique mutation in *clpX* have been identified. These mutations have been proven to cause resistance to ILE and ILF in mycobacteria through genome point mutation by gene editing, marking the first instance of such findings. ILE significantly impedes the proteolytic function of both the ClpC1P1P2 complex and ClpXP1P2 complex, representing the inaugural report on killing mycobacteria by targeting ClpX, highlighting the Clp complexes as promising potent targets, particularly through a dual-targeting strategy.

Keywords ClpC1, ClpX, Ilamycin E, Ilamycin F, Mycobacteria, Dual-targeting strategy

Introduction

Mycobacteria are classified into three primary categories: the *Mycobacterium tuberculosis* (Mtb) complex, *Mycobacterium leprae* and non-tuberculous mycobacteria (NTM). Among these, tuberculosis (TB), which is caused by Mtb, continues to pose a significant global public health threat, with the situation being exacerbated by the emergence of drug-resistant Mtb strains (Pfyffer, 2000; Miotto et al., 2018). Infections caused by NTM, such as *Mycobacterium abscessus* (Mab), are on the rise due to intrinsic resistance to almost all the existing antibiotics, and in several countries, the incidence of NTM infections has surpassed that of TB (Fedrizzi et al., 2017; Wu et al., 2018). Consequently, there is an urgent need to discover and develop new drugs with novel mechanisms of action against drug-resistant mycobacteria to effectively manage mycobacterial diseases.

The caseinolytic protease (Clp) proteolytic system in mycobacteria has recently emerged as a promising therapeutic target (Lee and Suh, 2016; Lupoli et al., 2018; Fraga et al., 2019; d'Andrea et al., 2022). This system is pivotal not only for maintaining intracellular protein quality but also for modulating responses to environmental stressors and contributing to the pathogenicity of virulent strains (Lupoli et al., 2018; Texier et al., 2021). It comprises multi-subunit protein complexes that facilitate intracellular protein degradation. In mycobacteria, the core complex of the hetero-tetradecamer Clp protease assumes a barrel-shaped structure, constructed from two rings, each composed of seven ClpP1 and seven ClpP2 peptidase subunits. The entry of substrates into the ClpP1P2 complex is stringently regulated and reliant on ATP-dependent AAA+ unfoldases (ClpX or ClpC1), which act as adaptors to facilitate substrate entry into the protease chamber through ATP hydrolysis (Akopian et al., 2012; Raju et al., 2012; d'Andrea et al., 2022). Both the Clp protease genes and the ATPase adaptor genes *clpX* and *clpC1* have been found essential for mycobacterial

survival (Sassetti et al., 2003; d'Andrea et al., 2022).

Many non-ribosomal natural cyclic peptides, such as ilamycins (also known as rufomycins), cyclomarins, and ecumicins, have been reported to possess antitubercular activities by targeting the ClpC1 component of the ClpC1P1P2 proteasome (Boshoff et al., 2024). However, aside from the mutations identified in the *clpC1* gene from spontaneous resistant mutants, robust genetic evidence is lacking. Although these compounds all disrupt protein metabolism through the Clp system, their mechanisms of action (MOAs) differ. For example, rufomycin decreases the proteolytic activity of the ClpP1P2 complexes by binding to ClpC1, interfering with its binding to ClpP1P2, while cyclomarin stimulates ClpC1's ATPase and promotes proteolysis by the ClpC1P1P2 proteasome (Schmitt et al., 2011; Choules et al., 2019). On the other hand, ecumicin stimulates the ATPase activity of ClpC1 but inhibit the proteolysis by ClpP1P2 (Gao et al., 2015). To the best of our knowledge, there are no reported anti-Mtb compounds targeting ClpX.

We previously reported that ilamycin E (ILE) and ilamycin F (ILF), synthesized by *Streptomyces atratus* SCSIO ZH16 isolated from the South China Sea, exhibited activities against Mtb (Ma et al., 2017). Particularly, ILE demonstrated superior activity against Mtb compared to other ilamycin components and the aforementioned compounds (Gavrish et al., 2014; Ma et al., 2017; Boshoff et al., 2024). However, their MOAs, activities against NTM and other non-mycobacterial pathogenic bacteria, and potential drug interactions remain to be elucidated. In this study, we have discovered that ILE and ILF kill Mtb by targeting both the ClpC1P1P2 and ClpXP1P2 complexes. This finding underscores the potential of Clp complexes as viable therapeutic targets, particularly when employing a dual-targeting approach.

Results

The selective and potent *in vitro* and *ex vivo* antimycobacterial activities of ILE/F

Mtb and 3 different NTM (Mab, *Mycobacterium marinum* (Mmr), *Mycobacterium smegmatis* (Msm) were selected to investigate the activities of ILE and ILF. These mycobacteria were chosen due to their clinical relevance and growth characteristics. Mab, a rapidly growing mycobacteria, is frequently associated with severe human infections (Victoria et al., 2021) and is known for its intrinsic antibiotic-resistant nature (Luthra et al., 2018). Mmr, a slowly growing mycobacteria, is closely related to Mtb (Stinear et al., 2008) but less virulent and serves as a model organism for Mtb studies (Shiloh and Champion, 2010). Msm is also utilized widely as a model organism due to its rapid growth, non-virulence and the availability of genetic tools (Shiloh and Champion, 2010).

ILE and ILF demonstrated significant inhibitory activities against Mtb, Mmr, and Msm with varying potencies (Table 1). Notably, ILE exhibited potent activity against Mab at a concentration of 1 μg/mL, whereas ILF only showed weak activity at 20 μg/mL, though they showed highly bactericidal activities against Mtb. This disparity in efficacy may stem from ILE and ILF structural differences and the unique cell wall permeabilities of each mycobacterial species (Jankute et al., 2014; Gutiérrez et al., 2018). Compared to rifampicin (RIF), ILE and ILF exhibited delayed antimicrobial

activities, initially displaying minor bacteriostatic effects on Mtb, with bactericidal activity emerging after six days of incubation (Fig. 1). Similar killing dynamics were observed for Mab, Mmr, and Msm (Fig. S1). The minimal inhibitory concentrations (MICs) of ILE against clinically isolated drug-resistant Mtb strains ranged from 0.01 to 0.05 μg/mL, which aligns with the laboratory standard Mtb $H_{37}Rv$ strain (Table 1). Synergistic effects were observed when combining ILE with RIF or the novel anti-TB drug TB47 (Lu et al., 2019) or combining ILF with isoniazid (INH) or TB47. Partial synergy was noted when ILE was paired with INH, ethambutol (EMB), clofazimine (CFZ), or bedaquiline (BDQ), and when ILF was combined with CFZ. Additive effects were observed when ILE was combined with streptomycin (STR), or ILF combined with EMB, STR or BDQ. No antagonism was detected between any of the selected drugs and either ILE or ILF. In mouse RAW264.7 macrophages, ILE effectively inhibited autoluminescent Mtb $H_{37}Rv$ (AlRv), with an MIC of 0.2 μg/mL. However, neither ILE nor ILF exhibited activity against common non-mycobacterial clinical isolates, with MICs exceeding 128 μg/mL (Table 1).

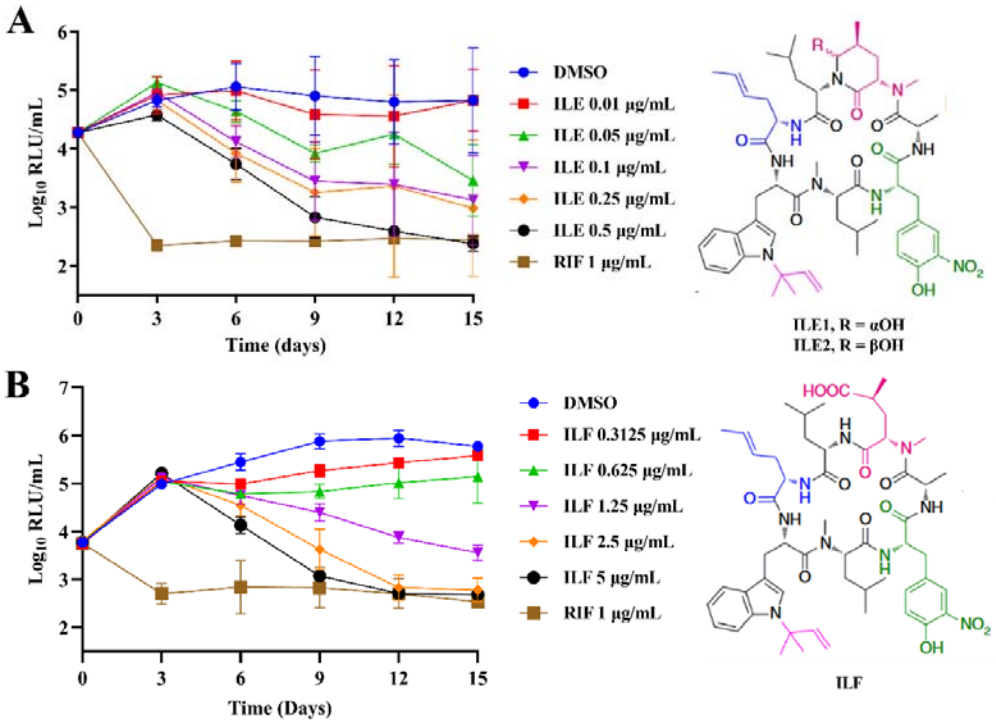

Figure 1. Time-kill curves of ILE and ILF against autoluminescent Mtb $H_{37}Ra$ (AlRa) and their structures. (A) Time-kill curves of ILE against AlRa and its structure. (B) Time-kill curves of ILF against AlRa and and its structure. The MIC_{lux} was defined as the lowest concentration that can inhibit > 90% relative light units (RLUs) compared with that from the untreated controls. DMSO, dimethyl sulfoxide, solvent control; RIF, positive control.

Mutation patterns in *clpC1* and/or *clpX* in ILE- or ILF-resistant Mtb, Mab, Msm, and Mmr mutants

The spontaneous mutation rate for producing ILE-resistant Mtb was approximately 2.5×10^{-9}, which is similar to that of rufomycin and lower than that of ecumicin and lassomycin, as well as RIF (Bergval et al., 2012; Gavrish et al., 2014; Gao et al., 2015; Choules et al., 2019). Whole genome sequencing (WGS) analysis revealed predominant mutations at P30 of ClpX and F80 of ClpC1 in ILE-resistant Mtb strains (Table 2). Similarly, ILE-resistant Mab exhibited mutations at the same site in ClpX and different sites in ClpC1, including F2, Q17, H77, L88, and an insertion between M1 and F2, resulting in an M1-FERF-F2 sequence (Table 2). However, ILE-resistant Mmr strains carried mutations exclusively in ClpC1 without any mutations in ClpX (Table 2). Additionally, ILF-resistant Msm mutants showed mutations in ClpC1 only, at F2, F5, F80, L88, I197, and an insertion between M1 and F2, leading to an M1-L-F2 sequence (Table 2), respectively. Cross-resistance between ILE and ILF was observed in all ILE- or ILF-resistant NTM mutants. These findings suggest that ILE and ILF may both target the ClpX and ClpC1, especially in Mtb and Mab.

Molecular docking of ILE to the N-terminal domains (NTD) of MtbClpC1 and MtbClpX

Based on the reported structure of MtbClpC1-NTD (Wolf et al., 2019) and the predicted structure of MtbClpX-NTD using AlphaFold2, we docked ILE to the MtbClpC1-NTD (Fig. 2A) and MtbClpX-NTD (Fig. 2B), respectively. The docking results indicate that the key residues involved in drug binding include the aforementioned mutation sites, namely Q17, H77, F80, and L88 in MtbClpC1-NTD, as well as P30 in MtbClpX-NTD. Given the structural similarity between ILE and ILF, and the observed cross-resistance, ILF likely binds ClpC1 and ClpX at similar binding sites.

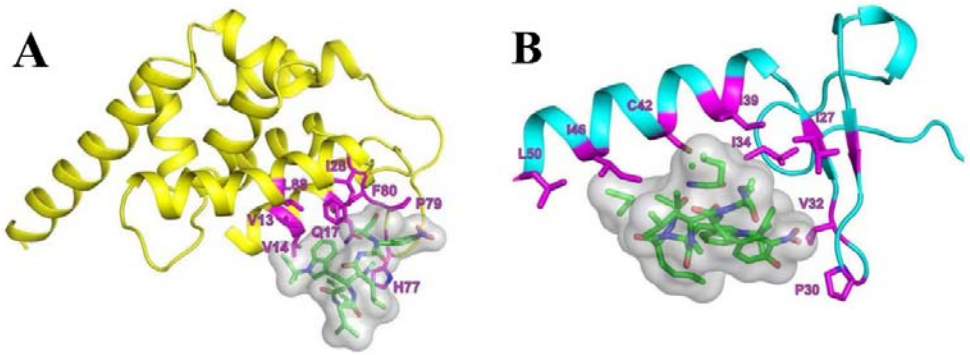

Figure 2. The graphical representation of crucial residues in the interaction between ILE and MtbClpC1-NTD as well as MtbClpX-NTD. (A) Crucial residues in the interaction between ILE and MtbClpC1-NTD. (B) Crucial residues in the interaction between ILE and MtbClpX-NTD. MtbClpC1-NTD, N-terminal domain of MtbClpC1 (residues 1–145); MtbClpX-NTD, N-terminal domain of MtbClpX (residues 1–112).

The sensitivity of Mab, Mmr or Msm overexpressing genes encoding subunit(s)

of Clp proteases to ILE or ILF

The wild-type (wt) genes *clpX*^{wt} and *clpC1*^{wt}, along with their mutant variants, were inserted into two extrachromosomal plasmids, p60A or pMVA, each bearing distinct resistance markers (Fig. S2). These genes were under the robust *hsp60* promoter to facilitate overexpression in autoluminescent strains of Mab (AlMab), Msm (AlMsm), and Mmr (AlMmr) (Yang et al., 2015; Liu et al., 2019b; Liu et al., 2020). Among these strains, only the AlMmr strain overexpressing ClpC1^{L88R} demonstrated resistance to both ILE and ILF when compared to the parent strain (Table 3). However, the overexpression of wild-type and mutated forms of ClpC1 or ClpX, as well as the concurrent overexpression of genes encoding the ClpC1P1P2 or ClpXP1P2 complexes in AlMab and AlMsm, did not alter their susceptibility to ILE or ILF. These findings are consistent with previous observations, suggesting that the overexpression of all mutated *clpC1* does not necessarily confer resistance to ClpC1-targeting compounds, and that efficacy varies across different mycobacterial species (Vasudevan et al., 2013).

The effect of *clpC1* or *clpX* editing in Mab and Msm on their sensitivities to ILE and ILF

Given the slower growth rate and the absence of efficient gene editing tools for Mtb compared to rapidly-growing mycobacteria such as Msm and Mab, we initially utilized these two NTM to validate the impact of ClpX or ClpC1 mutations observed on ILE and ILF resistance. Utilizing the newly developed CRISPR/Cpf1-mediated gene editing techniques (Yan et al., 2017; Wang et al., 2023), we introduced specific *clpC1* and *clpX* mutations into Mab and Msm, resulting in two Mab mutants (ClpC1^{wt} to ClpC1^{F2L}; ClpX^{wt} to ClpX^{P30H}) and three Msm mutants (ClpC1^{wt} to ClpC1^{F2C}, ClpC1^{wt} to ClpC1$^{M1\text{-}L\text{-}F2}$ and ClpC1^{wt} to ClpC1^{I197N}). These genetically modified strains displayed varying levels of resistance as summarized in Table 4.

Notably, the ClpX^{P30H} mutation in Mab conferred the highest level of resistance, with MICs exceeding 128 μg/mL for both ILE and ILF. The ClpC1^{F2L} mutation in Mab led to a more modest increase in resistance, elevating the MIC for ILE by eight times relative to the parent strain. The mutations ClpC1^{F2C} and ClpC1$^{M1\text{-}L\text{-}F2}$ in Msm both resulted in a greater than 4-fold increase in the MICs of ILE and ILF, compared to the parent strain. A comparative analysis of spontaneous mutants and gene-edited strains revealed that mutations at the F2 of ClpC1 in both Mab and Msm confer relatively low-level resistance to ILE and ILF, whereas the P30H mutation in Mab ClpX is associated with high-level resistance, underscoring its crucial role. It is noteworthy that the lack of impact of the Msm ClpC1^{I197N} mutation on ILE and ILF resistance may be attributed to its location outside NTD (residues 1-145) of ClpC1, suggesting that resistance is primarily driven by alterations within the NTD. Furthermore, the spontaneous mutant strain harboring *clpC1*^{I197N} also possessed *clpC1*^{F2S} (Table 2) which may be the principal factor contributing to ILE and ILF resistance.

The sensitivities of *clpX*- or *clpC1*-knocked down Mab or Msm strains to ILE or ILF

The knockdown of *clpX* or *clpC1* in Mab (Fig. 3A) and Msm (Fig. 3B) strains resulted in heightened sensitivity to ILE and ILF. Upon induction with anhydrotetracycline (aTc) in the absence of ILE or ILF, growth inhibition was observed in both the *clpX* or *clpC1* knockdown strains of Msm and Mab, highlighting the crucial role of these proteins in cellular proliferation. This finding corroborates previous reports on their essentiality in Msm and Mab (Bai et al., 2021; Rifat et al., 2021).

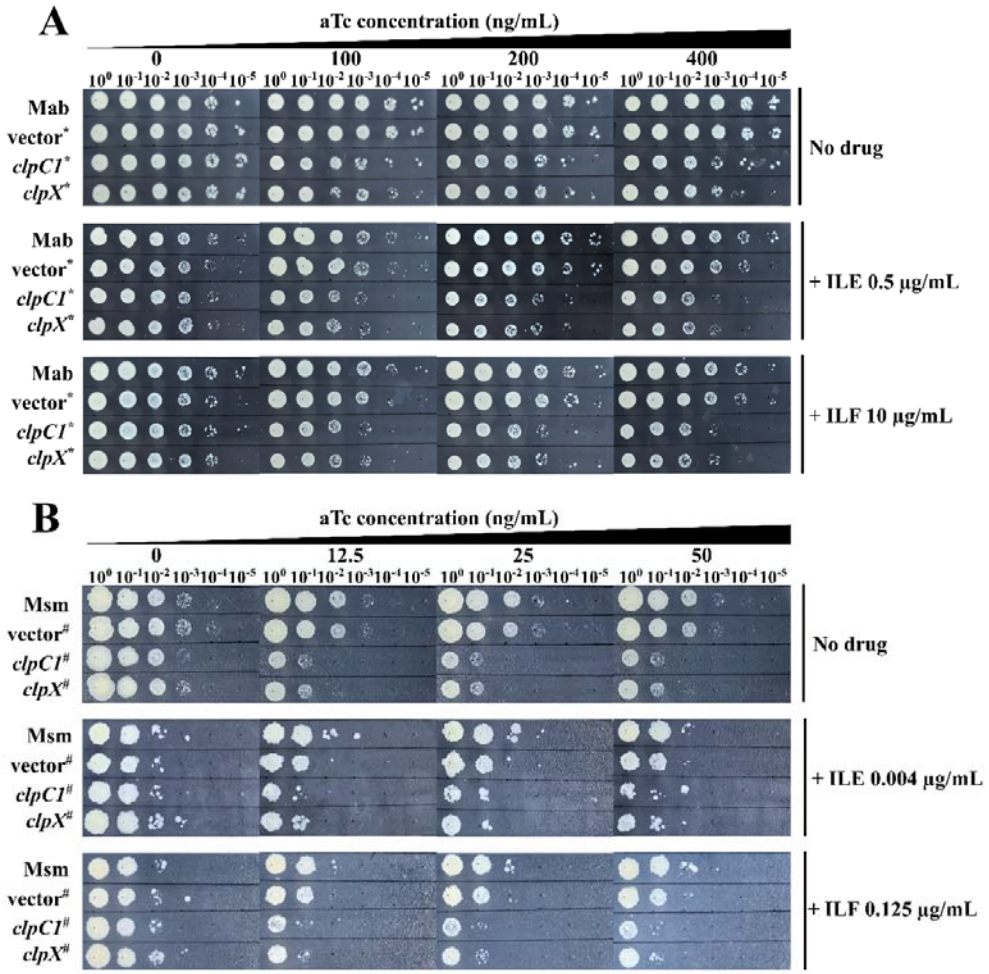

Figure 3. The impact of suppressing *clpX* or *clpC1* genes on the sensitivity of Mab and Msm to ILE or ILF. (A) The sensitivity of Mab to ILE or ILF upon gene suppression. (B) The sensitivity of Msm to ILE or ILF under similar conditions. aTc was served as the inducer for gene suppression. *, Mab strains contained varying plasmids: vector, a vector control with the empty plasmid pLJR962; *clpC1*, pLJR962-clpC1 for inducible inhibition of the *clpC1* gene; *clpX*, pLJR962-clpX for inducible inhibition of the *clpX* gene. #, Similarly, Msm strains were differentiated by the plasmids they harbored as that in Mab.

The interactions between ClpC1-NTD or ClpX and ILE or ILF

Since all mutations occurred within NTD of ClpC1 or that of ClpX across Mtb, Mab, Msm, and Mmr, and their ClpC1-NTD or the first 64 amino acids of the ClpX-NTD

(residues 1–112) sequences are identical (Figs. S3 and S4), we specifically expressed and purified the NTDs of ClpC1 and ClpX from Mtb. Subsequently, the interactions between the MtbClpC1-NTD or MtbClpX-NTD with ILE or ILF were examined by differential scanning fluorimetry (DSF). We discovered that ILE increased the melting temperature (Tm) of MtbClpC1-NTD from 78.5□ to 81.5□ (Fig. 4A), signifying a significant enhancement in thermal stability (ΔTm of 3□). Conversely, ILF marginally augmented the thermal stability of the MtbClpC1-NTD by merely 1□ (Fig. 4B) compared to ILE. The stronger affinity of ILE over ILF correlates with its lower MIC. These findings suggest potential interactions of ILE and ILF with MtbClpC1-NTD. However, we could not discern any alteration in the melting temperature of MtbClpX-NTD by ILE and ILF.

Nevertheless, it was evident that as the concentration of ILE or ILF increased, less ClpX protein underwent degradation (Figs. 4C and 4D) in a drug affinity responsive target stability (DARTS) assay, which was employed to identify small molecule targets previously (Gao et al., 2015; Pai et al., 2015). This implies that both ILE and ILF can bind to the ClpX, shielding it from proteolytic digestion by pronase. However, a significantly higher concentration of ILF is required compared to ILE in order to protect Mtb ClpX from degradation, suggesting a lower binding affinity of ILF with ClpX.

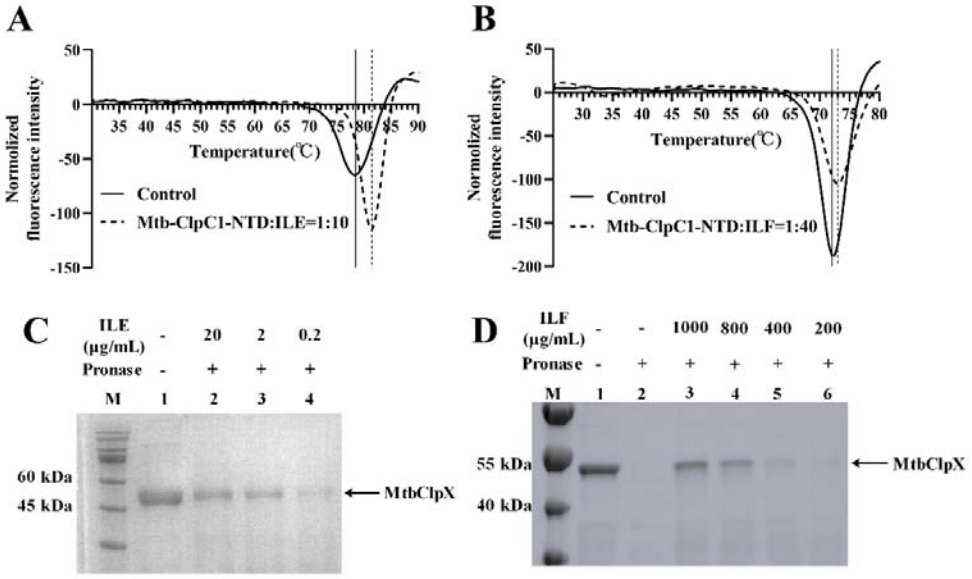

Figure 4. The interactions between MtbClpC1-NTD and either ILE or ILF, as well as the interactions between the MtbClpX and either ILE or ILF. (A) The melting curves of MtbClpC1-NTD in the presence of ILE are shown. (B) The melting curves of MtbClpC1-NTD in the presence of ILF are illustrated. Control, samples contained DMSO; Normalized fluorescence intensity refers to the fluorescence intensity normalized to the first time point after excitation for each well. (C) ILE protects wild-type MtbClpX from protease digestion, as analyzed by SDS-PAGE. Lanes: M, protein ladder; 1, MtbClpX without any treatment; 2 to 4, MtbClpX treated with different concentrations of ILE and digested by protease. (D) ILF protects wild-

type MtbClpX from protease digestion, as analyzed by SDS-PAGE. Lanes: M, protein ladder; 1, MtbClpX without any treatment; 2, MtbClpX digested by protease; 3 to 6, MtbClpX treated with different concentrations of ILF and digested by protease.

The impact of ILE on the proteolytic functions of the ClpC1P1P2 and ClpXP1P2 complexes, as well as its effect on the ATPase activities of ClpC1 and ClpX

Considering the stronger interactions observed between MtbClpC1-NTD and ILE compared to ILF, we focused our subsequent biochemical assays on evaluating ILE. We observed that ILE inhibited the proteolysis of the model substrate, fluorescein isothiocyanate (FITC)-casein, by ClpC1^{wt}P1P2 complex compared to the control group (Fig. 5A). However, the proteolytic activities of multiple mutant ClpC1P1P2 complexes remain unaffected at 10 μg/mL ILE compared to the control, with only partial inhibition noted at 20 μg/mL ILE (Figs. 5B-5E).

Previous studies have indicated that the adaptor SspB can efficiently recognize an *E. coli* tag, DAS+4, and successfully deliver the tagged protein to ClpXP1P2 in Msm (Kim et al., 2011). Therefore, we expressed the GFP-DAS+4 and *E. coli* SspB and observed a significant inhibition of ILE on the proteolytic activity of the ClpX^{wt}P1P2 complex during the hydrolysis of GFP-DAS+4 in the presence of SspB (Fig. 5F).

Additionally, we noted that ILE did not impact the ATP-dependent enzymatic activities of ClpC1 and ClpX, as no significant differences in ATPase activities were detected across varying ILE concentrations compared to controls (Fig. S5).

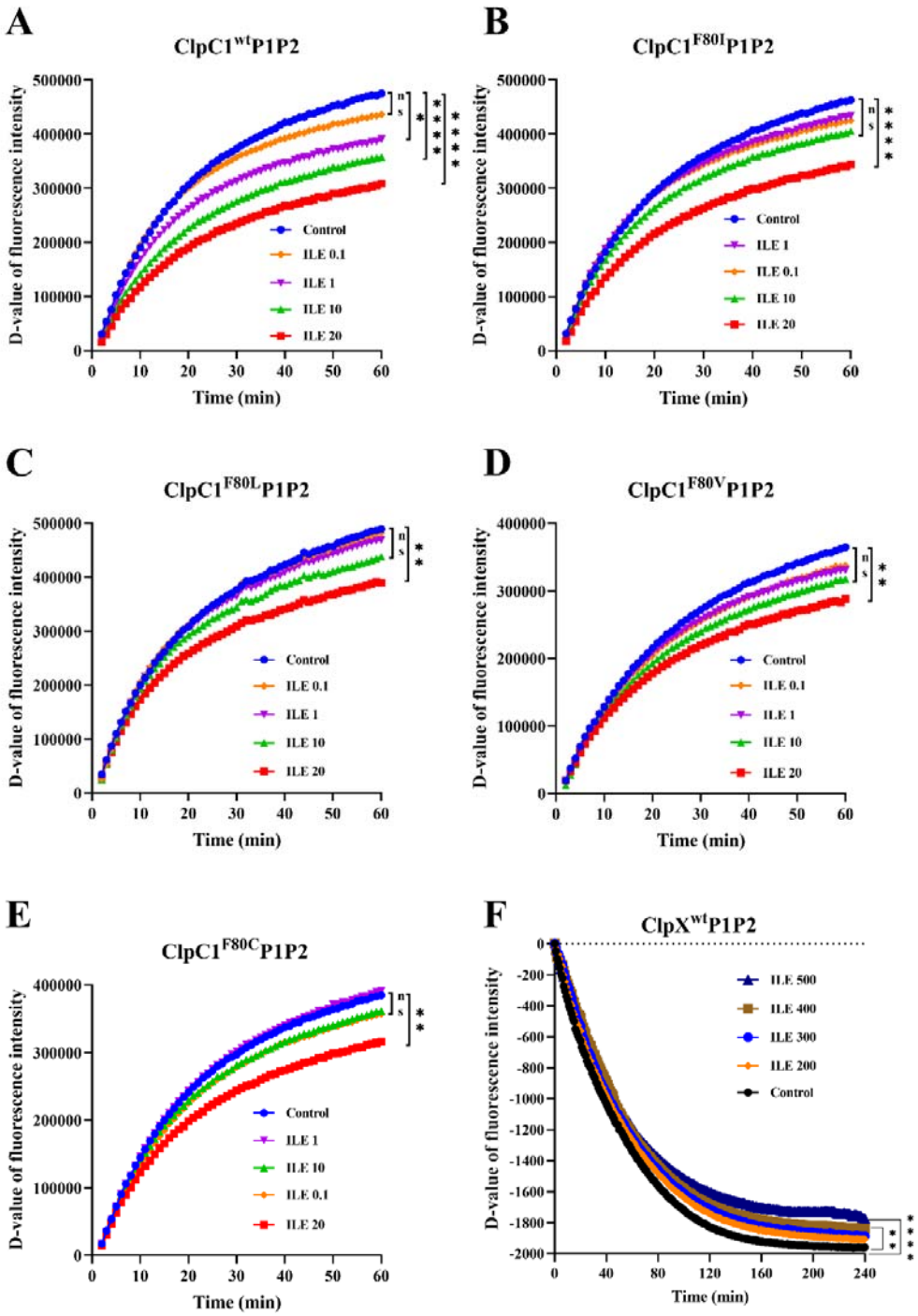

Figure 5. The proteolytic activities of the ClpC1P1P2 and ClpXP1P2 complexes in response to ILE treatment. (A-E) The proteolytic activities of various ClpC1P1P2 complexes in response to ILE treatment. (F) The proteolytic activities of the ClpXP1P2 complexes after ILE treatment. The formation of complexes was as follows: ClpC1^{wt}P1P2, ClpC1^{F80I}P1P2, ClpC1^{F80L}P1P2, ClpC1^{F80V}P1P2, and ClpC1^{F80C}P1P2 represent the assembly of wild-type and mutant ClpC1 with ClpP1

and ClpP2. The ClpXP1P2 complex is formed by the association of $ClpX^{wt}$ with ClpP1 and ClpP2. Numbers following the drug names indicate the working concentrations (μg/mL). DMSO was added as control. The D-value of fluorescence intensity represents the change in fluorescence intensity by subtracting the initial fluorescence intensity from the fluorescence intensity of subsequent detections. *, $P < 0.05$; **, $P < 0.001$; ****, $P < 0.00001$; ns, no significant difference, where $P > 0.05$.

The effect of ILE or ILF treatment on the morphology of Msm cells

To elucidate the bactericidal mechanisms of ILE and ILF, Msm was cultured with 0.125 μg/mL of ILE or 5 μg/mL of ILF for 15 hours. Notably, the cell lengths of Msm increased from 2.07 ± 0.48 μm to 5.95 ± 2.16 μm and 9.41 ± 2.40 μm following treatment with ILE and ILF, respectively (Fig. 6). In comparison to untreated Msm, ILE and ILF both induced a marked increase in cell length and a pronounced inhibition of cell division, as evidenced by the formation of division septa (Figs. 6B and C). This observation is consistent with the phenotype observed in Msm upon *clpX* gene silencing, and the established role of ClpX in regulating FtsZ assembly and Z-ring formation which are crucial processes for cell division in Mtb (Dziedzic et al., 2010; Bai et al., 2021).

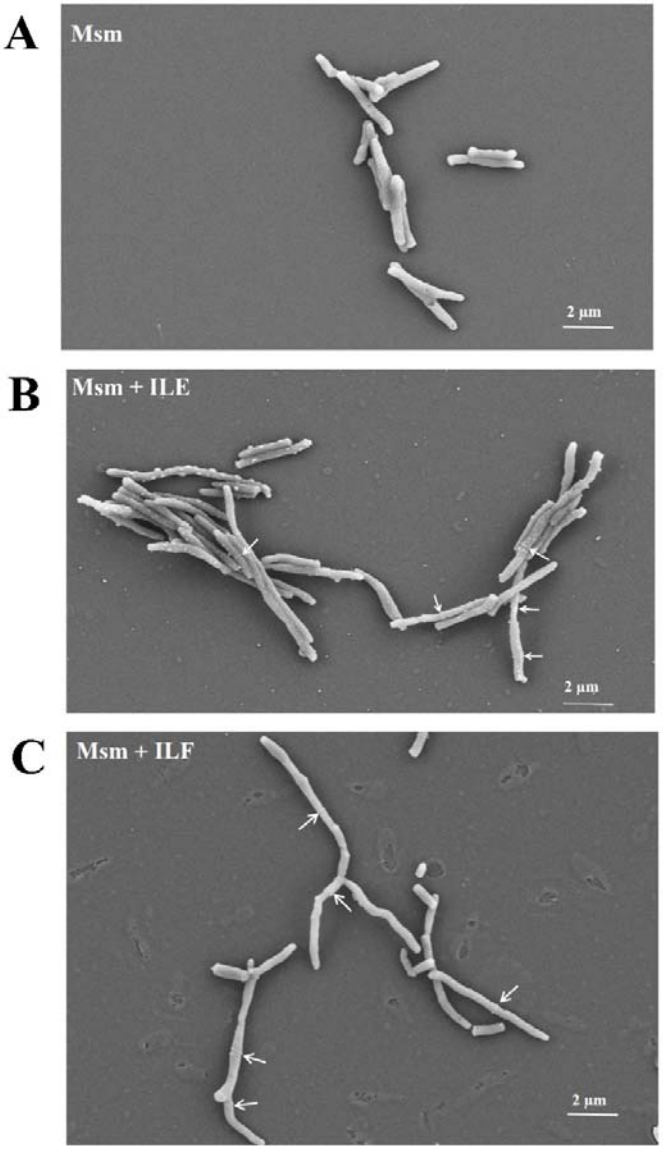

Figure 6. The cell morphology of Msm strains before or after treatment with ILE or ILF. (A) The cell morphology prior to any treatment. (B) The cell morphology of Msm treated with a concentration of 0.125 μg/mL ILE. (C) The cell morphology of Msm treated with a concentration of 5 μg/mL ILF. The white arrows highlight the division septa.

Proteomic signature of the Mtb treated with ILE

The proteomics of cells treated with ILE were investigated to understand the adaptive responses of Mtb during ILE treatment, thereby enhancing our understanding of its activity and MOA. A differential expression of proteins was noted post-treatment with ILE (Table S1). In comparison to non-treated cells, Mtb cells subjected to ILE exhibited an upregulation of proteins associated with protein synthesis, including various 50S and 30S ribosomal proteins such as RpsG, RpsS, RpmB, and RpmF. However, only RplR and RpsC displayed downregulation. Key sigma transcription

factors, which are essential for gene transcription, namely SigE, SigB, and SigL, were also upregulated. Notably, components of the toxin-antitoxin system, including toxin factors Rv0240 and Rv2142c, as well as antitoxins Rv0660c and Rv0748, were upregulated in response to ILE treatment. Conversely, no down-regulated components of either toxins or antitoxins were observed. This finding is consistent with previous reports suggesting that certain toxin-antitoxin proteins are targeted by the ClpXP1P2 complex (Texier et al., 2021). Surprisingly, ClpX was found to be downregulated, potentially leading to an accumulation of toxin-antitoxin proteins and contributing to the altered cell morphology in ILE-treated Mtb (Texier et al., 2021).

The expression of membrane proteins was significantly perturbed, with some experiencing increased expression while others showed a decrease. Proteins involved in the intermediary metabolism and respiration of Mtb, such as QcrA, QcrC, and CydD, were downregulated, indicating a potential impact of ILE on respiratory pathways. Changes in lipid metabolism-related proteins were also evident, including the upregulation of FadE9, FadE29, and FadD24, alongside the downregulation of FadD9, FadE6, FadE12, and FadE24. Furthermore, numerous membrane proteins (e.g., MmpL2, EccD5, EccE2) exhibited significant alterations in expression, whereas others like MmpS3, SecF, and TatA were downregulated in the presence of ILE.

Discussion

The study of natural cyclic peptides has emerged as a focal point in the current research on drugs against Mtb. In comparison to the reported cycloheptapeptides, ILE demonstrates superior anti-Mtb activity. Specifically, rufomycin I inhibited Mtb growth at a MIC of 60 nM by day 14 when tested with the autoluminescent Mtb strain, while ILE achieves an MIC of 48 nM (equivalent to 0.05 μg/mL) by day 15 (Fig. 1A) (Shetye et al., 2021). Moreover, the MIC of ILE is more than twice as low as those of cyclomarin A (100 nM), ecumicin (160 nM), and lassomycin (410 nM) reported (Gavrish et al., 2014; Boshoff et al., 2024). While these compounds exhibit activity against a range of NTM, only rufomycin I and ILE exhibit efficacy against Mab, indicating their potential as therapeutic agents for diseases caused by Mab (Choules et al., 2019).

Previously, the combination effects of cycloheptapeptides with anti-TB drugs had not been explored, leaving their potential as adjuvants to current TB therapies unresolved (Schmitt et al., 2011; Gavrish et al., 2014; Gao et al., 2015; Choules et al., 2019). Notably, our findings on combinatorial activity suggest that ILE and ILF have the potential to enhance the efficacy of existing anti-TB drugs, including INH, EMB, CFZ, BDQ, and TB47. Proteomic analysis indicated that ILE modulated the expression of four proteins (SigL, Ndh, FadE24, and Glf) associated with metabolic pathways affected by INH. Specifically, SigL and Ndh were significantly upregulated, whereas FadE24 and Glf were downregulated. SigL has been reported to regulate the expression of KatG, which is crucial for the activation of INH, and Ndh has been identified to influence the $NADH/NAD^+$ ratio, affecting INH-NAD formation (Sklar et al., 2010; Unissa et al., 2016; Hameed et al., 2018). INH-resistant Mtb has been found to carry mutations in FadE24 (Ramaswamy et al., 2003). Upregulation of Glf was hypothesized to contribute to INH resistance in Mtb either by binding to a

modified form of INH or by sequestering a factor such as NAD^+ required for INH activity (Chen and Bishai, 1998). Additionally, key proteins in the electron transport chain of Mtb, such as QcrA, QcrC, and CydD, were all downregulated after treatment with ILE. The QcrB protein is the target of the TB47 (Liu et al., 2019b; Gao et al., 2021). Furthermore, given the interchangeability of the two electron transfer chains, it was previously speculated that the inhibitory effect of the QcrB inhibitor TB47 on Mtb would be enhanced when the Cyt-bds complex containing CydD is inhibited (Liu et al., 2019b).

Although ILE and ILF have demonstrated potent activity against Mtb, their MOAs remained elusive (Ma et al., 2017). Previous studies had identified cyclic peptides that specifically target ClpC1 (Wolf et al., 2019). WGS and Sanger sequencing of spontaneous mutants resistant to ILE or ILF also identified ClpC1 as the primary target in Mtb, Mab, Msm, and Mmr. The mutations in ClpC1 found in ILE- or ILF-resistant mutants were similar to those reported in mutants resistant to known ClpC1-targeting cyclic peptides, with the exception of unique insertion mutations discovered between M1 and F2 in both Mab and Msm (Vasudevan et al., 2013; Gavrish et al., 2014; Gao et al., 2015; Choules et al., 2019). Prior research had primarily relied on indirect genetic validation of these mutations through overexpression (Vasudevan et al., 2013). With advancements in genetic manipulation tools for mycobacteria, we have directly confirmed the role of specific mutations, such as the F2L mutation in Mab, the F2C mutation and the newly discovered insertion mutation in Msm, in conferring resistance to ILE and ILF through gene editing for the first time.

Interestingly, no ClpX mutations had been reported in mutants resistant to these compounds (Gavrish et al., 2014; Gao et al., 2015; Choules et al., 2019). However, our findings indicate that ILE-resistant mutants harboring ClpX mutations also exhibit cross-resistance to ILF, suggesting that these two components of ilamycins may interact with multiple targets within the mycobacterial proteolytic machinery. This interaction could explain the superior activity of ILE against Mtb compared to previously reported compounds. Furthermore, we have directly confirmed that ClpX mutations can lead to high-level resistance to both ILE and ILF by gene editing. These observations suggest that certain cyclic peptide natural products, such as rufomycin I, may also target the ClpX protein. The selection of rufomycin I- and ecumicin-resistant mutants through stepwise inoculation on plates impregnated with increasing concentrations of compounds may have overlooked strains with high levels of resistance that acquired the ClpX mutation (Gao et al., 2015; Choules et al., 2019). Similarly, for lassomycin, only a limited number of resistant mutants with relatively low levels of resistance were obtained, potentially hindering the discovery of another target, ClpX (Gavrish et al., 2014). In the case of cyclomarin A, the target was identified using affinity chromatography and chemical proteomics. However, our results from DSF experiments suggest that ClpX protein may not have been isolated during the identification of cyclomarin A's targets due to its weaker affinity with ClpX (Vasudevan et al., 2013). Further by using DARTS, we were able to prove that both ILE and ILF can bind to ClpX. This study marks the first time that ClpX has

been identified as a target for discovering anti-Mtb drugs, paving the way for novel strategies in anti-mycobacterial drug development.

The MOA of ILE differs from ecumicin and lassomycin, which stimulate ClpC1 ATPase activity but hinder substrate degradation, as well as cyclomarin A, which activates both ATPase and proteolytic functions (Vasudevan et al., 2013; Gavrish et al., 2014; Gao et al., 2015). Notably, ILE does not influence the ATPase activities of ClpX and ClpC1. However, ILE inhibits the proteolytic activity of the ClpC1P1P2 complex, mirroring the MOA of rufomycin I (Choules et al., 2019). Prior investigations have not reported that these cyclic peptide compounds, particularly rufomycin I, could target the ClpX protein to affect the activity of the ClpXP1P2 complex (Vasudevan et al., 2013; Gavrish et al., 2014; Gao et al., 2015; Choules et al., 2019). Through using ClpX's adaptor SspB, we proved that ILE can inhibit the proteolytic activity of ClpXP1P2. Interestingly, a much higher concentration of ILE is required to inhibit ClpXP1P2 than ClpC1P1P2. This finding is consistent with the fact that a mutation in ClpX results in a higher level of resistance. In this study, we reported for the first time that natural products ILE and ILF can kill mycobacteria by simultaneously targeting ClpX and ClpC1, inhibiting the activities of both ClpC1P1P2 and ClpXP1P2 complexes (Fig. 7).

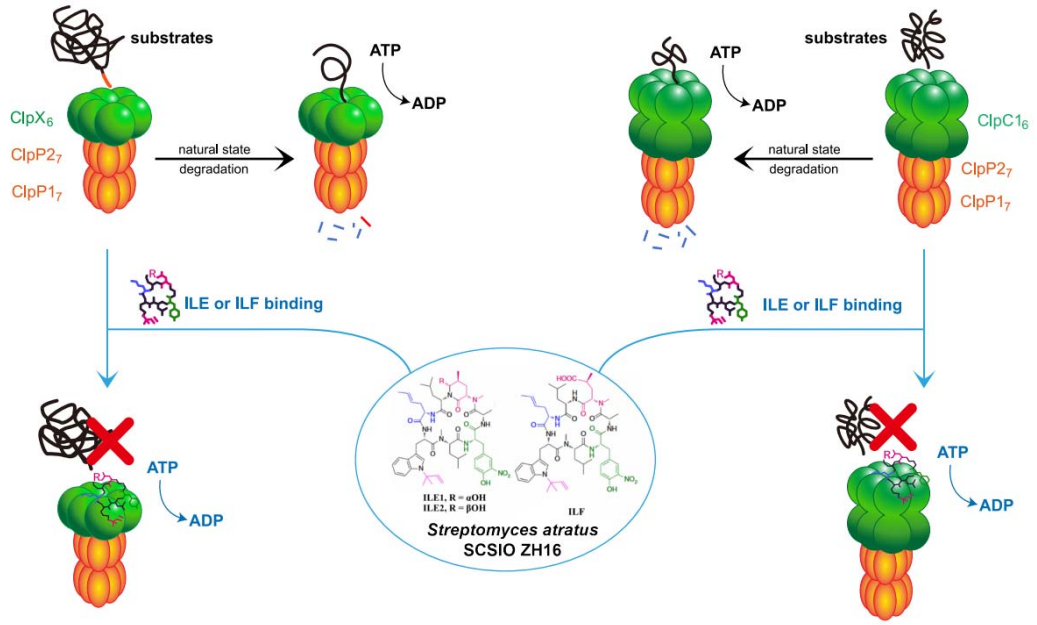

Figure 7. Schematic diagram of bactericidal mechanism of ILE and ILF. The hexameric ClpC1 or ClpX recognizes, unfolds, and translocates the dysfunctional protein into the chamber of the heptameric ClpP1P2 proteolytic complex, which is dependent on the ATPase activity of ClpC1 and ClpX (top). ILE and ILF can inhibit the proteolytic activity of the ClpC1P1P2 and ClpXP1P2 complexes by binding to ClpC1 and ClpX, while not affecting the ATPase activity of ClpC1 and ClpX (bottom).

However, we discovered that the mutant $ClpX^{P30H}$P1P2 complex was incapable of

degrading GFP-DAS+4. This may be attributed to the fact that the enhancement of ClpXP1P2 degradation by SspB requires an intact zinc binding domain (ZBD) in ClpX (residues 1-60) (Thibault et al., 2006). A mutation in P30, which is located in the hydrophobic surfaces of ZBD, may suppress the binding of SspB to ClpX, thereby preventing the delivery of the tagged protein to ClpXP1P2 complexes for degradation. Additionally, the roles of some *clpC1* mutation sites in ILE and ILF resistance remain unproven due to the inability to acquire corresponding gene-edited strains. Therefore, future studies should focus on identifying new substrates to detect the effect of mutated ClpX on the proteolysis ability of ClpXP1P2 and attempt to obtain the remaining *clpC1*-edited strains to confirm their roles in ILE and ILF resistance.

In summary, the potent and broad antimycobacterial activities of ILE and ILF underscore their potential for further development as effective agents against mycobacteria, especially drug-resistant strains. The cumulative evidence from this and related studies (Vasudevan et al., 2013; Gavrish et al., 2014; Gao et al., 2015; Choules et al., 2019) identify ClpC1P1P2 and, more importantly, ClpXP1P2 as promising targets for the development of antimycobacterial agents. A dual-targeting strategy that affects both simultaneously is a rational approach.

Materials and Methods

Bacterial strains and media

Bacterial strains used in this study are listed in Table S2. Mtb, Mmr, Mab, and Msm were grown in Middlebrook 7H9 broth supplemented with OADC (comprising 0.005% oleic acid, 0.5% bovine serum albumin, 0.2% dextrose, 0.085% catalase). Mab GZ002 and Msm mc^2155 were used as the wild-type strains (Chhotaray et al., 2020). For *E. coli*, *Enterococcus faecium*, *Staphylococcus aureus*, *Acinetobacter baumannii*, *Klebsiella pneumoniae* and *Pseudomonas aeruginosa*, cells were grown in Luria-Bertani (LB) broth.

MICs to mycobacteria determination

The MICs of ILE and ILF were determined using a cost-effective *in vitro* assay as previously described against a selectable marker-free autoluminescent Mtb $H_{37}Ra$ (AlRa), AlRv, AlMab, AlMsm and AlMmr (Zhang et al., 2012; Yang et al., 2015; Liu et al., 2019b; Liu et al., 2020). The MIC_{lux} was defined as the lowest concentration that could inhibit > 90% relative light units (RLUs) compared with that from the untreated controls (Zhang et al., 2012; Yang et al., 2015; Liu et al., 2019b; Liu et al., 2020). The MICs of the ILE were also determined by a well-established microplate alamar blue assay (MABA) against Mtb $H_{37}Ra$, $H_{37}Rv$ and nine clinical Mtb strains isolated from pulmonary TB patients hospitalized at Guangzhou Chest Hospital, Guangzhou, China (Liu et al., 2020). The MIC, as determined by the MABA method, is defined as the lowest concentration that prevents the color change from blue to pink, as observed with the naked eye.

MICs to non-mycobacteria determination

The MICs of ILE or ILF against *Enterococcus faecium*, *Staphylococcus aureus*, *Acinetobacter baumannii*, *Klebsiella pneumoniae* and *Pseudomonas aeruginosa* were

determined by observing the turbidity after 16 hours of incubation in LB broth at 37 °C. The MIC was defined as the lowest concentration, resulting in clarity in turbidity relative to that of untreated control cultures (Jiang et al., 2019; Wang et al., 2020; Tian et al., 2021).

Combined activity of ILE or ILF with other compounds *in vitro*

The combined activity of ILE or ILF with other compounds, such as INH, RIF, EMB, STR and TB47, was evaluated *in vitro* using the checkerboard method. The fractional inhibitory concentration index (FICI) was interpreted as follows: synergistic (FICI of ≤ 0.5), partially synergistic (0.5 < FICI < 1.0), additive (FICI = 1.0), indifferent (1.0 < FICI ≤ 4.0), and antagonistic (FICI > 4.0) (Liu et al., 2019a; Yu et al., 2020).

Activity in macrophage culture

The growth inhibition of AlRv in macrophage culture was assessed as previously described (Liu et al., 2019a). The cell density of mouse macrophages RAW264.7 was adjusted to 5×10^5 cells/mL. 100 μL of cells per well were added to 96-well plates and cultured overnight for adherence. The AlRv concentration was adjusted to 3×10^6 RLU/mL, and 100 μL of AlRv was added to each well. The plates were then incubated at 37 °C for 6 hours. The cells were washed three times with DMEM to remove non-phagocytosed AlRv and treated with DMEM containing amikacin (100 μg/mL) for 2 hours to eliminate the extracellular bacteria. The cells were washed twice with DMEM to remove residual amikacin. A total of 195 μL of DMEM containing 10% fetal bovine serum and 5 μL of the two-fold dilutions of various ILE concentrations were added to the cells. The mixture was incubated at 37 °C with 5% CO_2, and the RLUs were measured on days 1-5 or 7 of incubation. RIF (1 μg/mL) and dimethyl sulfoxide (DMSO) were used as positive and negative controls, respectively.

ILE- or ILF-resistant mutants

Broth cultures of AlRa, AlRv, AlMab, and AlMmr, having OD_{600} value of 0.6-1.3, were plated on 7H11 plates containing ILE at 0.1, 0.5, 2.5, 5, 10 or 20 μg/mL. Broth cultures of AlMsm (OD_{600} value of 0.6-1.3) were plated on 7H11 plates containing ILF at 10, 20 or 40 μg/mL. The bacterial colonies grown on the ILE- or ILF-containing plates were selected and grown in liquid culture for drug susceptibility testing to confirm the drug resistance phenotype.

WGS analysis

WGS analysis was conducted on the parent strains of Mtb, Mab, and a subset of the confirmed ILE-resistant mutants. The sequencing was performed by the Beijing Genomics Institute in China. Subsequently, the obtained reads were aligned with the reference genome sequence and compared to that of the parent strain. Mutations identified through WGS in the drug-resistant mutants were validated by amplifying and sequencing the *clpX* and *clpC1* genes using Sanger sequencing. Additionally, the *clpX* and *clpC1* genes from other ILE- or ILF-resistant mutants, including Mtb, Mab, Msm, and Mmr, were amplified and sequenced using Sanger sequencing (primer sequences are provided in Table S2).

Molecular docking analysis

To evaluate the binding affinities and interaction modes among ILE, MtbClpC1-NTD, and MtbClpX-NTD, we employed Autodock Vina 1.2.2, a computational protein-ligand docking software as referenced in the previous study (Morris et al., 2008). The structure of ILE was obtained from PubChem Compound (Wang et al., 2017). The 3D coordinates of MtbClpC1-NTD were retrieved from the Protein Data Bank (PDB) with PDB code 6CN8 and a resolution of 1.4 Å, while the structure of MtbClpX-NTD was predicted using AlphaFold2.

For the docking analysis, all protein and ligand files were converted to the PDBQT format; water molecules were excluded, and polar hydrogen atoms were supplemented. A grid box was positioned to envelop the domain of each protein, facilitating unrestricted molecular movement. The dimensions of the grid box were set to 30 Å × 30 Å × 30 Å, with a grid point spacing of 0.05 nm. The molecular docking experiments were executed using Autodock Vina 1.2.2, which is accessible at http://autodock.scripps.edu/.

Overexpression of *clpX* or *clpC1* in Mab, Mmr or Msm

clpC1^{wt}, *clpC1*^{mt} (mutated *clpC1*), *clpX*^{wt} and *clpX*^{mt} from Mtb, Mab, Mmr and Msm were amplified using primers detailed in Table S3 and subsequently cloned into the plasmid p60A or pMVA under the control of the *hsp60* promoter as depicted in Fig. S1. The plasmids were then transformed into AlMab, AlMmr, and AlMsm. Additionally, the *clpP1*, *clpP2* and *clpX* or *clpC1* of Mab were amplified from the genome of Mab^{wt} and inserted into the plasmid pMVA under the control of the *hsp70* or *hsp60* promoters to enable the simultaneous expression of ClpXP1P2 or ClpC1P1P2. The MICs of the recombinant strains to ILE or ILF were determined using the aforementioned protocols.

Silencing *clpX* or *clpC1* genes in Mab or Msm

The CRISPR-Cas9 system was employed for targeted gene silencing of *clpX* and *clpC1* as described in reference. Small guide RNAs (sgRNAs) of 20 base pairs were designed to target the coding regions of *clpX* and *clpC1* on their sense strands. The oligonucleotides were annealed and then ligated with linearized pLJR962 (Rock et al., 2017). Plasmids harboring sgRNAs against *clpX* or *clpC1*, along with the empty vector pLJR962 as a control, were introduced into Mab and Msm cells via electroporation (Table S3). The gene-silenced strains and the control strain carrying the empty vector were cultured, and the efficacy of gene silencing was assessed. 4 μL of ILE were added to each well of the 96-well microplate, resulting in a final concentration gradient ranging from 8 to 0.0313 μg/mL. Bacterial cultures were adjusted to an OD_{600} of approximately 0.5 and then diluted 1000-fold in 7H9 medium, with or without aTc.

The diluted bacteria were then divided into the experimental group (+ aTc 50 ng/mL) and the control group (- aTc). 196 μL of these two groups were then inoculated into the 96-well microplate separately. The microplates were incubated at 37 °C for 3 days. The MIC was defined as the lowest concentration that prevented visible bacterial growth. All experiments were conducted in triplicate and repeated independently at least twice.

Ten-fold serial dilutions of Mab^{wt} or Msm^{wt}, the control strain carrying the empty vector, and the gene-silenced strains were prepared after reaching an OD_{600} of approximately 0.9. For Mab, 1 μL of each dilution was spotted on plates containing either 0.25, 0.5, and 1 μg/mL ILE or 5, 10, and 20 μg/mL ILF with varying concentrations of aTc (0, 100, 200 and 400 ng/mL). For Msm, 1 μL of each dilution was spotted on plates containing either 0.004, 0.008, and 0.01625 μg/mL ILE or 0.125, 0.25, and 0.5 μg/mL ILF with varying concentrations of aTc (0, 12.5, 25 and 50 ng/mL). Control plates received 1 μL of each dilution with aTc alone. The plates were incubated at 37 °C for 3 days. The experiment was performed in triplicate and repeated twice.

CRISPR/Cpf1-mediated gene editing of *clpX* and *clpC1* genes in Mab and Msm

The CRISPR/Cpf1-associated recombination have been previously employed for gene editing in both Mab and Msm recently (Yan et al., 2017; Wang et al., 2023). Initially, the pJV53-Cpf1 plasmid was electroporated into Mab^{wt} and Msm^{wt} strains, resulting in the Mab::pJV53-Cpf1 and Msm::pJV53-Cpf1, respectively. Subsequently, crRNAs were designed to target specific 25 nucleotide sequences adjacent to the 5'-YTN-3' motif on the template strand of the target genes (Table S3). Oligonucleotides for crRNA expression were ligated into the pCR-zeo vector. These constructed vectors were then electroporated into the respective acetamide-induced cells of Mab::pJV53-Cpf1 or Msm::pJV53-Cpf1. For the induction of Cpf1 expression, aTc was added to 7H11 agar plates to achieve a final concentration of 200 ng/mL. These plates were cultured at 30 °C for 3-5 days. Individual colony was picked and screened to confirm successful editing at the target gene site via PCR and Sanger sequencing (primers listed in Table S3). The MICs of the edited strains to ILE and ILF were determined using the methods described earlier.

Expression and Purification of Proteins

The Mtb ClpP1 (residues 7-200) with a C-terminal Strep-II tag and ClpP2 (residues 13-214) with a C-terminal His_6-tag were expressed and purified. Briefly, *clpP1* and *clpP2* genes were inserted into the pETDuet-1 vector and overexpressed in *E. coli* BL21 (λDE3) in LB broth at 25 °C, following induction with 0.5 mM isopropyl β-D-1-thiogalactopyranoside (IPTG) for approximately 16 hours. Cells were resuspended and lysed; The target protein was subsequently purified via nickel affinity chromatography and eluted with the same buffer supplemented with 200 mM imidazole. Eluted fractions containing the target protein were loaded onto a Strep-II column. The target protein was eluted with the strep buffer containing 50 mM HEPES-KOH (pH 7.5), 150 mM KCl, 10 mM $MgCl_2$, 50 mM d-Desthiobiotin and 10% glycerol (v/v), before a final gel filtration using a Superose™ 6 increase 10/300 GL column (GE Healthcare) in SEC buffer (25 mM HEPES-KOH (pH 7.5), 150 mM KCl, 10 mM $MgCl_2$).

The sequence of $clpX^{wt}$ or $clpX^{P30H}$ was inserted into the pGEX-6P-1 vector, which had a His_6-tag at the C-terminus and an HRV 3C protease cleavage site. After induction for 18 hours at 16 °C, the cells were collected by centrifugation. The pellet

was then resuspended and lysed. After centrifugation, the supernatant was loaded onto a GST column and eluted. The eluent underwent digestion at 4 °C for 26 hours with enough HRV 3C protease. The fractions containing the target protein were then pooled, concentrated to 1 mL, and purified with a Superose™ 6 increase 10/300 GL column.

The sequence of *clpC1*^{wt}, its mutants (F80I/V/L/C), the gene encoding *gfp*-DAS+4 (AANDENYSENYADAS) or *E. coli sspB* was inserted into the pET-28a vector that had an N-terminal His_6-tag. The recombinant strains were cultured in LB broth at 37 °C until the OD_{600} reached 0.6-0.8. After 18 hours of induction with 0.5 mM IPTG at 18 °C, the pellet was suspended and lysed. Following the loading of the supernatant onto a Ni-NTA column, the proteins were washed and then eluted. The fractions were then pooled and loaded onto a Superose™ 6 increase 10/300 GL column.

The gene encoding MtbClpC1-NTD or MtbClpX-NTD was inserted into the pET-28a vector with a C-terminal His_6-tag and an HRV 3C protease cleavage site. The expression and purification methods of MtbClpC1-NTD and MtbClpX-NTD were consistent with the methods described above.

Differential scanning fluorimetry (DSF)

The binding of ILE or ILF to the MtbClpC1-NTD and MtbClpX-NTD was detected using DSF, following established protocols (Vivoli et al., 2014; Khadiullina et al., 2022). A 5 μM solution of either MtbClpX-NTD or MtbClpC1-NTD was incubated with varying concentrations of ILE or ILF (ranging from 12.5 to 400 μM), as well as DMSO for 30 minutes, subsequently mixed with Sypro Orange fluorescent dye. Fluorescence measurements were recorded using the CFX96 Real-Time System (Bio-rad), which involved heating 8-tube PCR Strips from 25 °C to 95 °C at a constant rate of 0.4 °C/minute. The excitation and emission filters were adjusted to wavelengths of 460 nm and 510 nm, respectively. Data collection was facilitated by the CFX Manager software, with analysis performed using GraphPad Prism version 8.3.0. To ensure accuracy, all measurements were performed in triplicate.

Drug affinity responsive target stability (DARTS) assay

DARTS was employed to detect the binding between ILE or ILF and Mtb ClpX, following well-established protocols (Gao et al., 2015; Pai et al., 2015). The ClpX concentration was determined using a BCA protein assay kit and adjusted to a total protein concentration of 0.5 mg/mL with 1 × TNC buffer (50 mM Tris-Cl pH 8.0, 50 mM NaCl, and 10 mM $CaCl_2$) for DARTS application. ClpX was divided into 19 μL aliquots and incubated with DMSO (as a control) or treated with different concentration of ILE or ILF. For ILE, final concentrations of 0.2, 2, and 20 μg/mL were added. For ILF, final concentrations of 200, 400, 800 and 1000 μg/mL were added. All mixed samples were then incubated at room temperature for 1 hour. Pronase (2 μL at 2.5 μg/mL) was then added to each sample, while 2 μL TNC buffer was added to the control group, and incubation continued for an additional hour at room temperature. Subsequently, 5 μL of 5 × SDS-PAGE loading buffer was added to the digested samples, and the mixtures were heated at 95 °C for 10 minutes to

terminate the digestion reaction. The sample proteins were then separated on 12% SDS-PAGE gels, stained with SimplyBlue SafeStain, and finally subjected to decolorization and photography.

Proteolytic activity assays of ClpC1P1P2 and ClpXP1P2

The proteolytic activities of ClpC1P1P2 and ClpXP1P2 were measured at 37 °C in black 96-well plates using a Multimode Plate Reader. For the ClpC1P1P2 proteolytic activity experiments, ILE was added at final concentrations of 0, 0.1, 1, 10, and 20 μg/mL in each well. A 100 μL reaction mixture was formulated with 2 μM ClpP1P2, 1 μM ClpC1, 2 mM ATP, and 2.5 μM FITC-casein. For the ClpXP1P2 proteolytic activity experiments, ILE was added at final concentrations of 0, 200, 300, 400, and 500 μg/mL in each well. A 100 μL reaction mixture was formulated with 0.2 μM ClpP1P2, 0.7 μM ClpX, 1 μM SspB, 2 mM ATP, 7 μM bortezomib as an activator, and 1 μM GFP-DAS+4.

The hydrolysis of FITC-casein and GFP-DAS+4 was continuously monitored at 535 nm (with excitation at 485 nm). Measurements were performed in triplicate.

ATPase activity assays of ClpC1 and ClpX

The ATPase activities of Mtb ClpC1 and ClpX were assessed using a free-phosphate detection assay with the Biomol Green reagent. To each well of a transparent 96-well plate, 5 μL of various concentrations of ILE (0, 0.08, 0.16, 0.31, 0.625, 1.25, 2.5, 5 and 10 μg/mL) was added. Subsequently, either ClpX or ClpC1 was diluted to a concentration of 0.1 μg/mL in the reaction mixture. 90 μL ClpC1 and ClpX were then added to a 96-well plate and incubated at 37 °C for 1 h. The reaction was initiated by adding 5 μL of 1 mM ATP to the reaction mixture, which was maintained at 37 °C for an additional hour. The final volume of the reaction mixture was adjusted to 100 μL. Post reaction, 100 μL of Biomol Green reagent was introduced to determine the amount of free phosphate. After a 30-minute incubation at room temperature, the resulting reaction product was measured at 620 nm using a Multimode Plate Reader. The concentration of free phosphate liberated from ATP by ClpX and ClpC1 was calculated using a standard curve based on the known concentration of free phosphate. Measurements were performed in triplicate.

Microscopy of ILE- or ILF-treated Msm

Treatment of exponentially growing Msm was conducted using 0.125 μg/mL ILE or 5 μg/mL ILF for a duration of 15 hours. The bacteria were immobilized with a 4% glutaraldehyde solution, followed by three washes and resuspension in phosphate-buffered saline (PBS). Bacterial suspensions were then applied to 5 mm cell slides, which were placed in a 24-well plate to dry naturally. Afterward, the cell slides underwent three additional PBS washes. The cell slides were subsequently soaked in ascending concentrations of ethanol solutions (70%, 80%, 90%, 100%) for 10 minutes each. Finally, the cell slides were dried using the critical point drying method and coated with an electrically-conducting material. Observations of bacterial morphology were made using a GeminiSEM 300 ultra-high resolution field emission cryo-scanning electron microscope.

Proteomic analysis

The AlRa cells were treated with 0.0125 μg/mL of ILE for 5 days in triplicate for 4D label-free phosphoproteomic analysis. To maintain comparable cell density between the untreated and ILE-treated groups, the untreated cells were diluted on the same day as the compound addition, prior to sample collection. The cells were resuspended and boiled for 20 minutes. Subsequently, the samples were sent to APTBIO (Shanghai, China) for proteomic testing and analysis.

To compare the abundance of phosphopeptides between the control and treatment samples, label-free quantification was performed with a minimum fold change of 1.5 to determine the differentially expressed phosphopeptides. Additionally, the student's *t*-test was employed to detect significant differences between the control and treatment samples, with $P < 0.05$ indicating significance. Functional category analysis was performed using Mycobrowser (https://mycobrowser.epfl.ch/). Protein functional annotation was conducted with DAVID (https://david.ncifcrf.gov/summary.jsp), and differentially expressed proteins were listed in Table S4 and S5.

Statistical analysis

Statistical analysis was conducted using GraphPad Prism 8.3.0. The unpaired *t*-test was applied to ascertain statistical significance, with $P < 0.05$ deemed significant.

Acknowledgments

We acknowledge the team of professor Yicheng Sun from the Institute of Pathogenic Biology, Chinese Academy of Medical Sciences for kindly sending the pJV53-Cpf1 and pCR-Zeo plasmids as the tool of gene editing. This work was supported by fundings from National Key R&D Program of China (2021YFA1300900), National Natural Science Foundation of China (81973372, 32300152, 82022067, 22037006), China Postdoctoral Science Foundation (2022M723164), Guangdong Provincial Basic and Applied Basic Research Fund (2022A1515110505, 2019B030302004), Grant of State Key Lab of Respiratory Disease (SKLRD-Z-202414, SKLRD-Z-202301), Open Program of Shen Zhen Bay Laboratory (SZBL2021080601006) and Nansha District Science and Technology Plan Project (NSJL202102).

Abbreviations

Mtb, *Mycobacterium tuberculosis*; NTM, non-tuberculous mycobacteria; TB, tuberculosis; Mab, *Mycobacterium abscessus*; Clp, caseinolytic protease; MOA, mechanism of action; ILE, ilamycin E; ILF, ilamycin F; Mmr, *Mycobacterium marinum*; Msm, *Mycobacterium smegmatis*; MIC, minimal inhibitory concentration; RIF, rifampicin; INH, isoniazid; EMB, ethambutol; CFZ, clofazimine; BDQ, bedaquiline; STR, streptomycin; AlRv, autoluminescent Mtb $H_{37}Rv$; AlRa, autoluminescent Mtb $H_{37}Ra$; WGS, whole genome sequencing; NTD, N-terminal domain; AlMab, autoluminescent Mab; AlMmr, autoluminescent Mmr; AlMsm, autoluminescent Msm; DSF, differential scanning fluorimetry; Tm, melting temperature; DARTS, drug affinity responsive target stability; FITC, fluorescein isothiocyanate; ZBD, zinc binding domain; RLU, relative light unit; MABA, microplate alamar blue assay; FICI, fractional inhibitory concentration index; wt, wild type; mt, mutated; sgRNA, small guide RNA; aTc, anhydrotetracycline; PDB, Protein

Data Bank; IPTG, isopropyl β-D-1-thiogalactopyranoside.

Conflict of interest

All authors declare that they have no conflicts of interest.

Author contributions

T. Z., J. J., and X. X. supervised the project. T. Z., Y. G., and C. F. designed the whole project and most of the experiments; J. M. and C. S. prepared and characterized the ilamycin E and ilamycin F; Y. G. and C. F. performed the susceptibility testing and resistant mutant screening; B. Z. and J. J. contributed to molecular docking simulation; C. F., X. T., and J. H. constructed overexpression and gene-editing strains and performed the susceptibility testing; C. F. and X. H. performed the gene-silencing experiments; Y. G. and B. Z. contributed to protein expression and mode of action experiments; C. F. and H. Z. contributed to the microscopy results; Y. G. performed the statistical analysis; Y. G., C. F., and T. Z. wrote the manuscript; HMA. H., J. M., J. L., X. C., N. Z., X. X., J. J., and T. Z. revised the manuscript.

Data availability

All data are available in the main text or the supplementary materials.

References

Akopian T, Kandror O, Raju RM, et al. The active ClpP protease from *M. tuberculosis* is a complex composed of a heptameric ClpP1 and a ClpP2 ring. EMBO J 2012;31:1529-1541.

Bai J, Chi M, Hu Y, et al. Construction and biological characteristics of ClpC and ClpX knock-down strains in *Mycobacterium smegmatis*. China Biotechnology 2021;41:13-22.

Bergval I, Kwok B, Schuitema A, et al. Pre-existing isoniazid resistance, but not the genotype of *Mycobacterium tuberculosis drives* rifampicin resistance codon preference in vitro. PLoS ONE 2012;7:e29108.

Boshoff HI, Malhotra N, Barry III CE, et al. The antitubercular activities of natural products with fused-nitrogen-containing heterocycles. Pharmaceuticals (Basel) 2024;17:211.

Chen P, and Bishai WR. Novel selection for isoniazid (INH) resistance genes supports a role for NAD+-binding proteins in mycobacterial INH resistance. Infect Immun 1998;66:5099-5106.

Chhotaray C, Wang S, Tan Y, et al. Comparative analysis of whole-genome and methylome profiles of a smooth and a rough *Mycobacterium abscessus* clinical strain. G3 (Bethesda) 2020;10:13-22.

Choules MP, Wolf NM, Lee H, et al. Rufomycin targets ClpC1 proteolysis in *Mycobacterium tuberculosis* and *M. abscessus*. Antimicrob Agents Chemother 2019;63:e02204-02218.

d'Andrea FB, Poulton NC, Froom R, et al. The essential *M. tuberculosis* Clp protease is functionally asymmetric in vivo. Sci Adv 2022;8:eabn7943.

Dziedzic R, Kiran M, Plocinski P, et al. *Mycobacterium tuberculosis* ClpX interacts with FtsZ and interferes with FtsZ assembly. PLoS ONE 2010;5:e11058.

Fedrizzi T, Meehan CJ, Grottola A, et al. Genomic characterization of nontuberculous mycobacteria. Sci Rep 2017;7:45258.

Fraga H, Rodriguez B, Bardera A, et al. Development of high throughput screening methods for inhibitors of ClpC1P1P2 from *Mycobacteria tuberculosis*. Anal Biochem 2019;567:30-37.

Gao W, Kim J, Anderson JR, et al. The cyclic peptide ecumicin targeting ClpC1 is active against *Mycobacterium tuberculosis* in vivo. Antimicrob Agents Chemother 2015;59:880-889.

Gao Y, Hameed HMA, Liu Y, et al. Ultra-short-course and intermittent TB47-containing oral regimens produce stable cure against Buruli ulcer in a murine model and prevent the emergence of resistance for *Mycobacterium ulcerans*. Acta Pharm Sin B 2021;11:738-749.

Gavrish E, Sit CS, Cao S, et al. Lassomycin, a ribosomally synthesized cyclic peptide, kills *Mycobacterium tuberculosis* by targeting the ATP-dependent protease ClpC1P1P2. Chem Biol 2014;21:509-518.

Gutiérrez AV, Viljoen A, Ghigo E, et al. Glycopeptidolipids, a double-edged sword of the *Mycobacterium abscessus* complex. Front Microbiol 2018;9:1145.

Hameed HA, Islam MM, Chhotaray C, et al. Molecular targets related drug resistance mechanisms in MDR-, XDR-, and TDR-*Mycobacterium tuberculosis* strains. Front Cell Infect Microbiol 2018;8:114.

Jankute M, Grover S, Birch HL, et al. Genetics of mycobacterial arabinogalactan and lipoarabinomannan assembly. Microbiol Spectr 2014;2:MGM2-2013.

Jiang H, Gao Y, Zeng S, et al. One-step engineering of a stable, selectable marker-free autoluminescent Acinetobacter baumannii for rapid continuous assessment of drug activity. J Microbiol Biotechnol 2019;29:1488-1493.

Khadiullina R, Mirgayazova R, Davletshin D, et al. Assessment of thermal stability of mutant p53 proteins via differential scanning fluorimetry. Life (Basel) 2022;13:31.

Kim JH, Wei JR, Wallach JB, et al. Protein inactivation in mycobacteria by controlled proteolysis and its application to deplete the beta subunit of RNA polymerase. Nucleic Acids Res 2011;39:2210-2220.

Lee H, and Suh JW. Anti-tuberculosis lead molecules from natural products targeting *Mycobacterium tuberculosis* ClpC1. J Ind Microbiol Biotechnol 2016;43:205-212.

Liu P, Yang Y, Tang Y, et al. Design and synthesis of novel pyrimidine derivatives as potent antitubercular agents. Eur J Med Chem 2019a;163:169-182.

Liu Y, Gao YM, Liu JX, et al. The compound TB47 is highly bactericidal against *Mycobacterium ulcerans* in a Buruli ulcer mouse model. Nat Commun 2019b;10:524.

Liu Y, Tan Y, Islam MM, et al. Assessment of clofazimine and TB47 combination activity against *Mycobacterium abscessus* using a bioluminescent approach. Antimicrob Agents Chemother 2020;64:e01881-01819.

Lu XY, Williams Z, Hards K, et al. Pyrazolo[1,5-]pyridine inhibitor of the respiratory cytochrome complex for the treatment of drug-resistant tuberculosis. ACS Infect

Dis 2019;5:239-249.
Lupoli TJ, Vaubourgeix J, Burns-Huang K, et al. Targeting the proteostasis network for mycobacterial drug discovery. ACS Infect Dis 2018;4:478-498.
Luthra S, Rominski A, and Sander P. The role of antibiotic-target-modifying and antibiotic-modifying enzymes in *Mycobacterium abscessus* drug resistance. Front Microbiol 2018;9:2179.
Ma J, Huang H, Xie Y, et al. Biosynthesis of ilamycins featuring unusual building blocks and engineered production of enhanced anti-tuberculosis agents. Nat Commun 2017;8:391.
Miotto P, Zhang Y, Cirillo DM, et al. Drug resistance mechanisms and drug susceptibility testing for tuberculosis. Respirology 2018;23:1098-1113.
Morris GM, Huey R, and Olson AJ. Using autodock for ligand□receptor docking. Curr Protoc Bioinf 2008;24:8.14. 11-18.14. 40.
Pai MY, Lomenick B, Hwang H, et al. Drug affinity responsive target stability (DARTS) for small-molecule target identification. Methods Mol Biol 2015;1263:287-298.
Pfyffer G. Drug-resistant tuberculosis: resistance mechanisms and rapid susceptibility testing. Schweiz Med Wochenschr 2000;130:1909-1913.
Raju RM, Unnikrishnan M, Rubin DH, et al. *Mycobacterium tuberculosis* ClpP1 and ClpP2 function together in protein degradation and are required for viability in vitro and during infection. PLoS Pathog 2012;8:e1002511.
Ramaswamy SV, Reich R, Dou S-J, et al. Single nucleotide polymorphisms in genes associated with isoniazid resistance in *Mycobacterium tuberculosis*. Antimicrob Agents Chemother 2003;47:1241-1250.
Rifat D, Chen L, Kreiswirth BN, et al. Genome-wide essentiality analysis of *Mycobacterium abscessus* by saturated transposon mutagenesis and deep sequencing. Mbio 2021;12:e0104921.
Rock JM, Hopkins FF, Chavez A, et al. Programmable transcriptional repression in mycobacteria using an orthogonal CRISPR interference platform. Nat Microbiol 2017;2:1-9.
Sassetti CM, Boyd DH, and Rubin EJ. Genes required for mycobacterial growth defined by high density mutagenesis. Mol Microbiol 2003;48:77-84.
Schmitt EK, Riwanto M, Sambandamurthy V, et al. The natural product cyclomarin kills *Mycobacterium tuberculosis* by targeting the ClpC1 subunit of the caseinolytic protease. Angew Chem, Int Ed Engl 2011;50:5889-5891.
Shetye GS, Choi KB, Kim CY, et al. In vitro profiling of antitubercular compounds by rapid, efficient, and nondestructive assays using autoluminescent *Mycobacterium tuberculosis*. Antimicrob Agents Chemother 2021;65:e0028221.
Shiloh MU, and Champion PAD. To catch a killer. What can mycobacterial models teach us about *Mycobacterium tuberculosis* pathogenesis? Curr Opin Microbiol 2010;13:86-92.
Sklar JG, Makinoshima H, Schneider JS, et al. *M. tuberculosis* intramembrane protease Rip1 controls transcription through three anti□sigma factor substrates. Mol Microbiol 2010;77:605-617.

Stinear TP, Seemann T, Harrison PF, et al. Insights from the complete genome sequence of *Mycobacterium marinum* on the evolution of *Mycobacterium tuberculosis*. Genome Res 2008;18:729-741.

Texier P, Bordes P, Nagpal J, et al. ClpXP-mediated degradation of the TAC antitoxin is neutralized by the SecB-like chaperone in *Mycobacterium tuberculosis*. J Mol Biol 2021;433:166815.

Thibault G, Yudin J, Wong P, et al. Specificity in substrate and cofactor recognition by the N-terminal domain of the chaperone ClpX. Proc Natl Acad Sci U S A 2006;103:17724-17729.

Tian X, Gao Y, Wang S, et al. Rapid visualized assessment of drug efficacy in live mice with a selectable marker-free autoluminescent *Klebsiella pneumoniae*. Biosens Bioelectron 2021;177:112919.

Unissa AN, Subbian S, Hanna LE, et al. Overview on mechanisms of isoniazid action and resistance in *Mycobacterium tuberculosis*. Infect Genet Evol 2016;45:474-492.

Vasudevan D, Rao SP, and Noble CG. Structural basis of mycobacterial inhibition by cyclomarin A. J Biol Chem 2013;288:30883-30891.

Victoria L, Gupta A, Gómez JL, et al. *Mycobacterium abscessus* complex: a review of recent developments in an emerging pathogen. Front Cell Infect Microbiol 2021;11:659997.

Vivoli M, Novak HR, Littlechild JA, et al. Determination of protein-ligand interactions using differential scanning fluorimetry. J Vis Exp 2014:e51809.

Wang S, Yu W, Liu Z, et al. Rapid, serial, non-invasive quantification of *Pseudomonas aeruginosa* in live mice with a selectable marker-free autoluminescent strain. Biosens Bioelectron 2020;165:112396.

Wang S, Zhang J, Hameed HMA, et al. Amino acid 17 in QRDR of Gyrase A plays a key role in fluoroquinolones susceptibility in mycobacteria. Microbiol Spectr 2023;11:e0280923.

Wang Y, Bryant SH, Cheng T, et al. Pubchem bioassay: 2017 update. Nucleic Acids Res 2017;45:D955-D963.

Wolf NM, Lee H, Choules MP, et al. High-resolution structure of ClpC1-rufomycin and ligand binding studies provide a framework to design and optimize anti-tuberculosis leads. ACS Infect Dis 2019;5:829-840.

Wu ML, Aziz DB, Dartois V, et al. NTM drug discovery: status, gaps and the way forward. Drug Discov Today 2018;23:1502-1519.

Yan M, Yan H, Ren G, et al. CRISPR-Cas12a-assisted recombineering in bacteria. Appl Environ Microbiol 2017;83:e00947-00917.

Yang F, Njire MM, Liu J, et al. Engineering more stable, selectable marker-free autoluminescent mycobacteria by one step. PLoS ONE 2015;10:e0119341.

Yu W, Chiwala G, Gao Y, et al. TB47 and clofazimine form a highly synergistic sterilizing block in a second-line regimen for tuberculosis in mice. Biomed Pharmacother 2020;131:110782.

Zhang T, Li SY, and Nuermberger EL. Autoluminescent *Mycobacterium tuberculosis* for rapid, real-time, non-invasive assessment of drug and vaccine efficacy. PLoS

880 ONE 2012;7:e29774.

Tables

Table 1. The ILE and ILF spectrum of activities

Strains or drug combinations	ILE MIC (μg/mL)	ILF MIC (μg/mL)	FICI
AlRa	0.05†	1.25†	-
AlRv	0.05†	ND	-
AlMsm	0.0625†	2.5†	-
AlMab	1†	20†	-
AlMmr	0.08†	0.625†	-
$H_{37}Rv$	0.025‡	2.5‡	-
K11*	0.025-0.05‡	ND	-
K12*	0.025‡	ND	-
K13*	0.01‡	ND	-
K14*	0.01‡	ND	-
K16*	0.05‡	ND	-
K17*	0.01‡	ND	-
K18*	0.025-0.05‡	ND	-
K19*	0.01‡	ND	-
K20*	0.05‡	ND	-
Staphylococcus aureus	> 128	> 128	-
Acinetobacter baumannii	> 128	> 128	-
Enterococcus faecium	> 128	> 128	-
Klebsiella pneumoniae	> 128	> 128	-
Pseudomonas aeruginosa	> 128	> 128	-
ILE + RIF	-	-	0.3125†
ILE + INH	-	-	0.625†
ILE + EMB	-	-	0.5625†
ILE + STR	-	-	1†
ILE + CFZ	-	-	1†
ILE + BDQ	-	-	0.62†
ILE + TB47	-	-	0.3125†
ILF + RIF	-	-	1.0625†
ILF + INH	-	-	0.3125†
ILF + EMB	-	-	1†
ILF + STR	-	-	1†
ILF + CFZ	-	-	0.63†
ILF + BDQ	-	-	1†
ILF + TB47	-	-	0.3125†

*Clinical resistant Mtb; †MICs obtained by detection of relative light units; ‡MICs obtained by the microplate alamar blue assay (MABA); -Not applicable; ND, not detected.

Table 2. Mutations of ClpC1 and ClpX in ILE- and ILF-resistant mutants

Strains No.	MICs (μg/mL)		Mutation			
	ILE	ILF	ClpC1	*clpC1*	ClpX	*clpX*
Mtb^{R1*}	0.625	-	-	-	P30H	CCC→CAC
Mtb^{R2*}	20	-	F80I	TTT→ATT	P30H	CCC→CAC
Mtb^{R3*}	20	-	F80V	TTT→GTT	P30H	CCC→CAC
Mtb^{R4*}	0.1	-	F80I	TTT→ATT	-	-
Mtb^{R5*}	0.1	-	F80V	TTT→GTT	-	-
Mtb^{R6*}	0.1	-	F80L	TTT→CTT	-	-
Mtb^{R7*}	20	-	F80C	TTT→TGT	-	-
Mab^{R1*}	> 128	> 128	-	-	P30H	CCC→CAC
Mab^{R2*}	4	> 128	F2L	TTC→TCC	-	-
Mab^{R3*}	4	> 128	M1-FERF-F2	Ins: TTCGA GAGATTC	-	-
Mab^{R4*}	4	> 128	Q17R	CAA→CGA	-	-
Mab^{R5*}	> 128	> 128	H77D	CAC→GAC	-	-
Mab^{R6*}	> 128	> 128	L88R	CTG→CGG	-	-
Mmr^{R1*}	1	4	F2L	TTC→TCC	-	-
Mmr^{R2*}	10	40	H77D	CAC→GAC	-	-
Mmr^{R3*}	10	40	L88R	CTC→CGC	-	-
Msm^{R1†}	0.5	20	F2S	TTT→TCT	-	-
Msm^{R2†}	0.25	10	F2C	TTT→TGT	-	-
Msm^{R3†}	1	20	M1-L-F2	Ins: GTT	-	-
Msm^{R4†}	1	10	F5I	TTT→ATT	-	-
Msm^{R5†}	0.5	40	F80S	TTC→TCC	-	-
Msm^{R6}†	0.25	10	L88P	CTC→CCC	-	-
Msm^{R7†}	0.25	20	L88R	CTC→CGC	-	-
Msm^{R8†}	0.25	10	F2S; I197N	TTT→TCT; ATC→AAC	-	-

*Resistant mutants selected from ILE-containing plates; †Resistant mutants selected from ILF-containing plates; Ins, insertion; Underlines indicate mutated bases; - showed no mutation.

Table 3. MICs of ILE and ILF against AlMmr strains overexpressing ClpC1 variants

Strains	MICs (μg/mL) / (fold change)	
	ILE	ILF
AlMmr^{wt}	0.08	0.625
AlMmr::ClpC1^{wt}	0.08 / (1)	0.625 / (1)
AlMmr::ClpC1^{L88R}	0.625 / (8)	5 / (8)
AlMmr::ClpC1^{F2L}	0.08 / (1)	0.625 / (1)
AlMmr::ClpC1^{H77D}	0.08 / (1)	0.625 / (1)

Table 4. MICs of ILE and ILF against gene edited strains and corresponding spontaneous mutants

Strains	Amino acid change	MICs (μg/mL) / (fold change)	
		ILE	ILF
Mab^{wt}	/	1	20
Mab^{R2*}	ClpC1^{wt} to ClpC1^{F2L}	4 / (4)	> 128 / (> 6)
Mab-C1^{F2L}	ClpC1^{wt} to ClpC1^{F2L}	8 / (8)	> 128 / (> 6)
Mab^{R1*}	ClpX^{wt} to ClpC1^{P30H}	> 128 / (> 128)	> 128 / (> 6)
Mab-X^{P30H}	ClpX^{wt} to ClpC1^{P30H}	> 128 / (> 128)	> 128 / (> 6)
Msm^{wt}	/	0.0625	2.5
Msm^{R2†}	ClpC1^{wt} to ClpC1^{F2C}	0.25 / (4)	10 / (4)
Msm-C1^{F2C}	ClpC1^{wt} to ClpC1^{F2C}	0.5 / (8)	20 / (8)
Msm^{R3†}	ClpC1^{wt} to ClpC1$^{M1-L-F2}$	1 / (16)	20 / (8)
Msm-C1$^{M1-L-F2}$	ClpC1^{wt} to ClpC1$^{M1-L-F2}$	0.25 / (4)	16 / (6.4)
Msm^{R8†}	ClpC1^{wt} to ClpC1^{F2S} ClpC1^{wt} to ClpC1^{I197N}	0.25 / (4)	10 / (4)
Msm-C1^{I197N}	ClpC1^{wt} to ClpC1^{I197N}	0.0625 / (1)	2.5 / (1)

*Resistant mutants selected from ILE-containing plates; †Resistant mutants selected from ILF-containing plates; -C1 or -X means ClpC1 or ClpX was edited.